Received: 29 March 2020 | Revised: 20 September 2020 | Accepted: 29 October 2020

IET Electrical Systems in Transportation

DOI: 10.1049/els2.12009

The Institution of Engineering and Technology WILEY

ORIGINAL RESEARCH PAPER

Experimental characterisation of active and non-active harmonic power flow of AC rolling stock and interaction with the supply network

Andrea Mariscotti[1,2]

[1]ASTM Sagl, Chiasso, Switzerland

[2]DITEN, University of Genova, Genova, Italy

Correspondence:
Andrea Mariscotti, DITEN, University of Genova, Via Opera Pia 11A, Genova, Italy.
Email: andrea.mariscotti@unige.it

Abstract

In AC electrified railways, there is a significant exchange of power at fundamental and harmonics in quite dynamic conditions. Harmonic patterns of AC rolling stock and railway networks are analysed in terms of active and non-active power flow, relating it to the characteristic of the network and to operating conditions, synthesised in the fundamental current intensity and speed. Herein, it is shown that correlation and clustering can separate distortion terms of internal and external origin also without a priori information. The use of harmonic power terms (product of voltage and current components) shows improved robustness with respect to the analysis of the voltage and current components alone.

1 | INTRODUCTION

It is generally recognized that reactive power and harmonic distortion are responsible for increased losses in the feeding system, from which the many regulatory standards, especially for public and industrial networks [1,2]. Considering AC railways, besides relevant non-active power terms, it was demonstrated in Refs. [3–5] that some harmonics can contribute to the active power flow. This is confirmed for variable speed drives [6–10], which are the main harmonic source on-board. Auxiliary on-board converters are also relevant, especially because of higher distortion (e.g. diode rectifier front end), visible in low traction conditions.

Rolling stock harmonic emissions are assessed and analysed for a variety of purposes: first of all prevention of interference to signalling, directly conducted or by induction [11,12], and more recently for assessment of power and energy consumption [3–5,13] [14], all carried out in a single-train perspective. Thus information on network and its quantities is limited to what can be measured at the line-pantograph interface. This may be seen as a restriction compared with other industrial applications, which see several interconnected Power Measurement Units and significant efforts to model and identify network response and propagation, especially for smart grids [15,16]. It is noted that an electrified railway is a continuously changing network with moving loads in quite dynamic conditions, and that the single-point measurement approach suites the vast range of rolling stock from different operators and manufacturers travelling within it. A metro conversely is an application with a known fleet that moves in a defined and delimited environment; partially networked solutions might be implemented for example at the Automatic Train Operation level. Metros are generally singly owned and accounting and fair billing are then purely formal. In addition, metros are DC supplied, with less relevant harmonic power terms, as confirmed by the preliminary analysis in Ref. [3].

The technological progress in the field of power conversion offers faster, lighter, more compact and more efficient converters with emissions spread farther over the frequency axis [17,18]. At the same time, electric transportation will reduce headway, packing more densely vehicles and trains, featuring faster and smarter dynamics [19]. Smart and microgrids have anticipated this tendency: supraharmonics have come into play beyond the 'usual' harmonics [20,21], with issues of network resonance also for small-size networks. Railways feature resonance at lower frequency, relevant for induction, interference and voltage stability [11,12,17,18]. Traction current harmonics undergo also a significant phase rotation with diversified propagation and interaction between vehicles [22]. In general, the harmonic spectrum of a vehicle in

a real traffic scenario will feature components of internal and external origin, where the on-board power circuit behave as a nonlinear distorting circuit or simply as a passive load.

Focusing on the significance of harmonic power and its impact on energy consumption and its metering, it is observed that the target uncertainty of EN 50463-2 [13] is a fraction of %, and it was demonstrated that harmonics altogether can bring a fraction of the fundamental active power of the same order [3–5], and that the harmonic non-active power is much larger. This means that the amplitude of harmonic power terms and their variability during train operation are a relevant factor for the uncertainty budget of the power and energy consumption and for reactive power impact in general. Although it is true that rolling stock input distortion is at all affected by the system timetable, when an optimization strategy changes intervals of traction, coasting, cruising and braking, correspondingly harmonic patterns and harmonic power will change, shifting in time or space along the line.

The analysis is carried out with experimental data collected in a single-train perspective [23].

2 | POWER QUANTITIES DEFINITION

Power quantities are introduced using IEEE Std. 1459 [24]. The total apparent power in non-sinusoidal conditions results from the multiplication of the two vectors of voltage and current at the pantograph, expressed as vectors of harmonic components: the order h is referred to fundamental pulsation ω, V_h and I_h are the amplitudes and α_h and β_h are the phases of the hth voltage and current component, respectively.

$$v_p = V_0 + \sqrt{2}\sum_h V_h \sin(h\omega t - \alpha_h) \tag{1a}$$

$$i_p = I_0 + \sqrt{2}\sum_h I_h \sin(h\omega t - \beta_h) \tag{1b}$$

Active and non-active power terms may be conveniently separated as in Refs. [25] and [26]:

- active power terms for the fundamental P_1 and harmonics P_h (resulting from the product of voltage and current components of the same order) are shown in (2);
- non-active power terms, encompassing reactive and distortion terms, resulting from multiplication of harmonics of different orders and the fundamental or dc component (that for AC railways may be neglected), as in (3).

$$p_a = \sum_h V_h I_h \cos\vartheta_h [1 - \cos(2h\omega t - 2\alpha_h)] \tag{2}$$

$$\begin{aligned} p_q = &-\sum_h V_h I_h \sin\vartheta_h \sin(2h\omega t - 2\alpha_h) \\ &+2\sum_m \sum_{m\neq n} V_m I_n \sin(m\omega t - \alpha_m)\sin(n\omega t - \beta_n) \\ &+V_0\sum_h I_h \sin(h\omega t - \beta_h) + I_0\sum_h V_h \sin(h\omega t - \alpha_h) \end{aligned} \tag{3}$$

where:

- the first term is the harmonic reactive power Q_h;
- the second term is a set of mixed products defining the distortion power D_h and involving both fundamental and harmonics; this term differs from that defined in IEEE Std. 1459 (D_H), that includes Q_h.

The objective is the characterisation of active and non-active power in terms of amplitude and distribution, compared with the fundamental terms:

- Active power terms at fundamental and harmonics can be summed, all contributing to the total active power

$$P_t = P_1 + \sum P_h \tag{4}$$

- Non-active power terms should be considered in terms of absolute value, to indicate the amount of exchanged power; reactive Q and distortion D power terms can then be summed together to get the total non-active power N_t. N_t may be determined as quadratic difference of total apparent power $S_t = V_{rms}I_{rms}$ and total active power P_t. N_t corresponds to the Fryze's fictitious power:

$$N_t = \sqrt{S_t^2 - P_t^2} \tag{5}$$

An example with a fundamental and three harmonics (total $n = 4$) for both voltage and current vectors is shown in Figure 1, using colours and height to suggest the pairing of components leading to non-active power terms: their number increases significantly with n (as $n + n(n-1)/2$, with the '/2' accounting for duplicated terms due to symmetry).

3 | ROLLING STOCK AND NETWORK DATA

Trains are characterised by harmonic patterns caused by the various non-linear loads on-board: waveform distortion and thus harmonic amplitude and distribution are different depending on the operating conditions. Differences may be observed for example between traction and braking (occurring through the same four-quadrant converters, 4QCs, in ac rolling stock) or during coasting and at standstill (when distortion is increased by the contribution of auxiliaries). For both situations, normative requirements to limit harmonics are still not fully addressing the problem: the EN 50388 [27] focuses only on the fundamental to define the 'power factor', although the prEN 50388-1 (draft of 2017, [28]) clearly separates the displacement factor from the power factor, the latter correctly including harmonics, but no limits are given, indicating the need for a compatibility study.

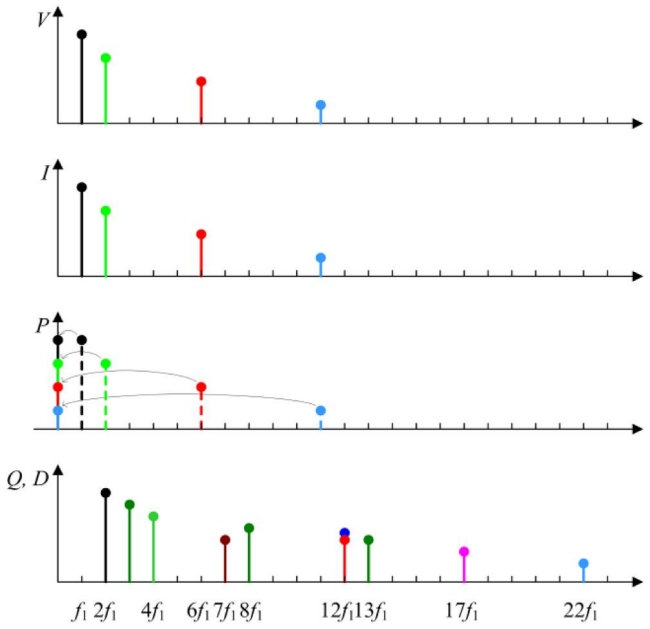

FIGURE 1 Active and non-active power components resulting from the combination of voltage and current harmonics

Partial cancellation of some components is in principle possible in the presence of more than one instance of the same model of rolling stock: not such an uncommon scenario if we consider that regional and commuter trains of the same operator are probably pulled by the same type of locomotive, as well as a fleet of high-speed trains is composed by lots of few different models. The harmonic components from the rolling stock undergo phase rotation whilst propagating along the traction line [22], overlapping within the same supply section, that for a 16.7 Hz system may be quite long, whereas in general for 50 Hz systems is limited to about 30–50 km.

Pantograph voltage and current waveforms (v_p and i_p) sampled and arranged in a dataset [23] with tags to indicate power absorption and speed as overall indication of rolling stock operating conditions, distinguishing traction, braking, coasting and standstill (this colour notation is used in the spectra of Figure 2: traction in red, braking in blue, coasting in black and standstill in green). Each short record (called 'snippet') has duration of five fundamental cycles, keeping harmonics well separated with frequency resolution of one fifth the fundamental: spectra V_p and I_p are calculated using Discrete Fourier Transform with a window T of 300 ms for the 16.7 Hz and 100 ms for the 50 Hz system. The selected time window is in line with the fastest time step adopted for electromechanical simulation [29,30], indicating that an almost steady-state assumption may be made for train kinematics and mechanical quantities. The snippets were extracted from continuous recordings every 2 s. The original data were sampled at 50 kS/s, ensuring sufficient oversampling even at the highest harmonics covered by this analysis, set to 5 kHz in agreement with previous works [3–5]. Hann window is used for spectral leakage.

The data refer to the following trains and networks:

- Switzerland: Romanshorn—Zurich—Brig with a Re460 locomotive (5.6 MW nominal power) in normal service; the switching frequency of the 4QC traction converter is 800 Hz resulting from four interleaved GTO converters each with 200 Hz switching frequency;
- Germany: Hamburg—Dortmund—Frankfurt with ICE-S train during test runs, whose power drive is similar to that of the ICE2, so based on GTO technology;
- France: Paris—Lyon with a TGV Dasye EMU (9.28 MW total nominal power) during test runs; the power chain of TGV Duplex series has diode rectifiers featuring a GTO power factor control and thyristors inverters.

The typical V_p and I_p spectra are shown in Figure 2 as a reference for the discussion of the power indexes in Section 4 and for the interpretation of results in Section 5.

Both systems feature a prevalent distortion of odd harmonics, with the exception of significant, but dispersed, values on the second and fourth harmonics. The third voltage harmonic is significant in all systems and is explained in Section 5.1. For France, the amplitude of harmonics is consistently above or close to 1000 V_{rms} up to about 2000 Hz, about 3 times larger than 16.7 Hz systems, once weighted by the respective nominal voltages [31]; also the second harmonic is larger and more dispersed, peaking occasionally (about 5% of time) to relevant values. The current spectrum for the Swiss case shows a consistent presence of loco harmonic signature between the 37th (617 Hz) and the 59th (983 Hz) harmonics. Other components at 2000 Hz are known to be due to other trains on the same line section, and possibly the components at about 1300 Hz. Similarly for Germany there are about five recognisable harmonic clusters at about 700, 1100, 1350, 1650 and 2000 Hz. For France, the recognisable harmonic clusters are at 1750, 2500 and 4000 Hz; the peak at 4850 Hz visible in the voltage spectrum may be the result of voltage amplification due to line resonance [17] [18].

4 | POWER FLOW INDEXES

4.1 | Basic quantities

Harmonic power terms can be evaluated and analysed by defining suitable basic indexes that focus on a single component using the framework set forth in Section 2. A combination of power components normalized by overall power terms is considered in the following.

As shown in Section 2 and Figure 1, each harmonic has a clearly defined active power P_h and reactive power Q_h (at twice the frequency), whereas the distortion power terms are related to pairs of components (m and n, including

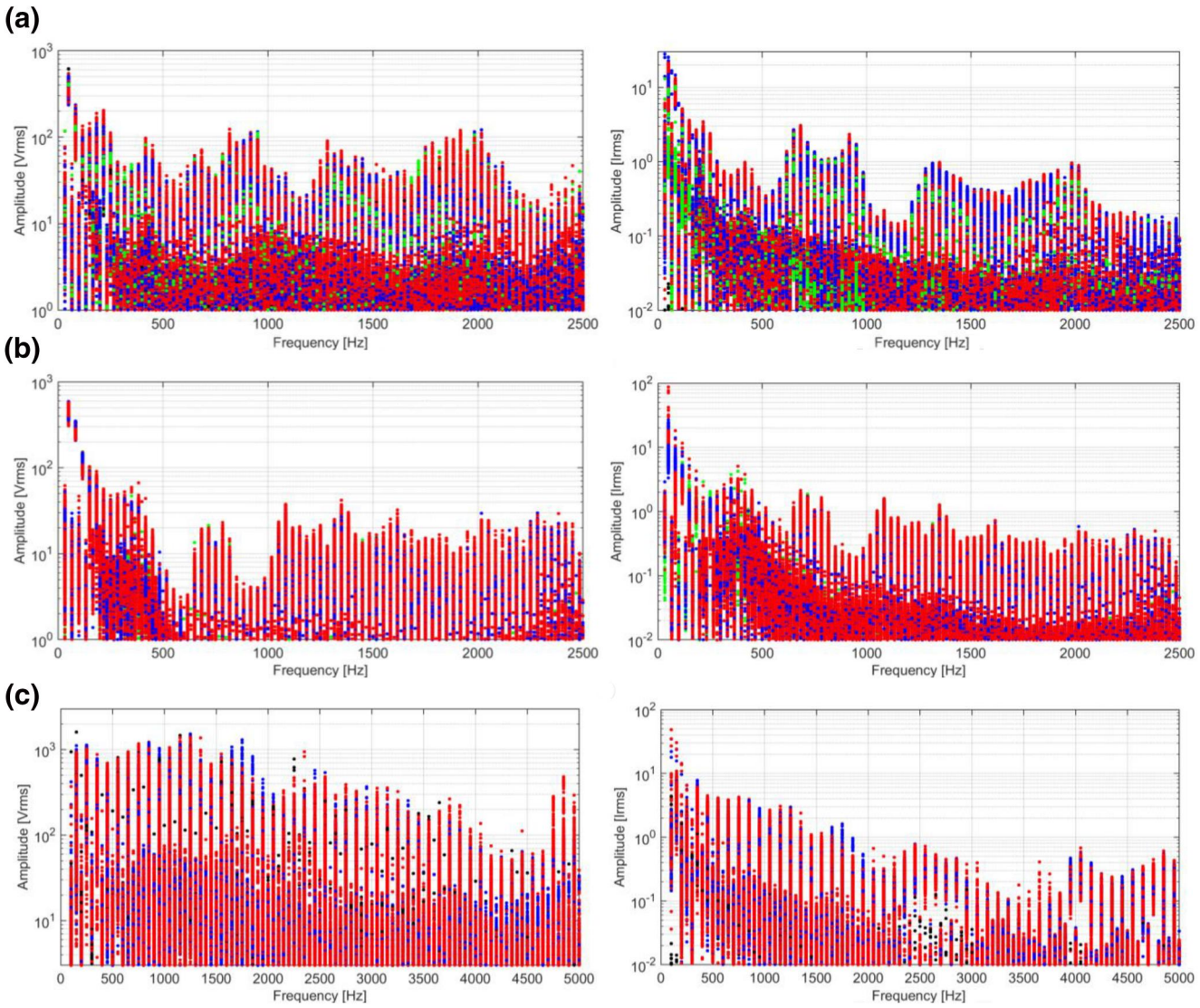

FIGURE 2 Harmonic spectrum of V_p and I_p (traction in red, braking in blue, coasting in black and standstill in green): (a) 16.7 Hz system (Switzerland), (b) 16.7 Hz system (Germany), (c) 50 Hz system (France) [23].

fundamental and harmonics). Invoking (3) half of each D_{mn} term may be assigned to each one of the two components m and n of the pair, although it is difficult to apply this rule when the fundamental is involved ($m = 1$), because the new D_{mn} term would add to the existing Q_1, modifying the definition of the non-active power at the fundamental from 'reactive' only to 'reactive + distortion'. For this reason it is opted to assign the resulting D_{1n} only to the harmonic n. For the interpretation of Q_h opinions are mixed, maintaining that isolating Q_h from the non-active harmonic power is groundless: without discussing it, we simply state that isolating Q_h is convenient to define the harmonic power displacement factor $d_h = P_h/S_h + j\ Q_h/S_h$.

The simple harmonic active power P_h well describes the flow of energy into and from the rolling stock, and may be considered a valid index, as discussed in Ref. [26], together with various distortion power indexes as single-point harmonic producer indicators. Active and non-active power terms may be also displayed as a fraction of the respective fundamental quantities or of the global values, as used in Ref. [3].

4.2 | Enhanced representations

Elaborations of basic indexes are considered to identify, visualise and track the harmonic signature of rolling stock, separating its harmonic components from those related to other rolling stock items and in general network distortion.

The harmonic active power flow P_h, also named Active Power Indicator [26], is quite useful to identify harmonics involved in the transfer of energy: both its statistics (e.g. percentiles) and the direction of flow (sign of P_h) are effective to display and track distortion power [5].

The introduced power displacement factor d_h or better the pair P_h–Q_h (to include the information of intensity) can be

displayed in polar coordinates and lend itself to clustering and separation of operating modes.

Similarly, V_h and I_h plotted in a Lissajous diagram give the amplitude of a complex quantity, the instantaneous impedance, $\xi_h = V_h/I_h$, with similar approach, but less robust to noise and local variations. Conversely, plotting the complex pattern of I_h components allows spotting out the modulation typical of static converters.

The power quantities discussed in Section 2 can all be evaluated using correlation and similarity with quantities taken to represent the operating conditions: in the present case, the rms of I_p, I_{rms} (a non-negative quantity), or the fundamental I_1 (including rms information and sign), and the speed s.

P_h–Q_h and V_h–I_h diagrams allow visual interpretation, evaluating the degree of clustering between different operating conditions (o.c.) and time intervals (t.i.): for a consistent relationship with a specific o.c., it is expected that the cluster shape repeats in different t.i.. External sources are expected to be uncorrelated and to change within the same o.c., although it must be noted that the input impedance of the rolling stock is in general lower during traction, so a slight amplification of current components (and thus of power terms) of external origin is expected. Criteria are clarified with examples in the next section.

5 | RESULTS FOR 16.7 AND 50 HZ SYSTEMS

The experimental data of the 16.7 and 50 Hz systems are used to analyse and discuss the characteristics of the identified quantities and representations.

5.1 | Active power flow

The largest harmonic active power P_h components are plotted in Figure 3 and Figure 4 for the 16.7 Hz systems, considering time intervals with traction, braking and coasting phases. The sign of P_h, P_h, is shown in red when directed into the loco, in blue when to the outside of it.

In Figure 3, we may observe that the second harmonic pulls significant active power almost in correspondence of blank intervals of very small I_{rms} values, characterised by very large distortion, and for this reason discarded from the traction/braking classification. The third harmonic pulls or pushes active power almost synchronized with traction and braking. The third harmonic is influenced by different factors: it is a network voltage harmonic and it is a by-product of deviations from the sinusoidal reference in 4QCs with a low switching frequency [9], but it is also the fundamental frequency for auxiliaries operating at 50 Hz, not at the 16.7 Hz traction frequency. Also the fifth and seventh are synchronised, but with opposite behaviour: harmonic active power enters the loco during braking and leaves it during tractioning. The low-order harmonics are in general prevalent; on-board converter

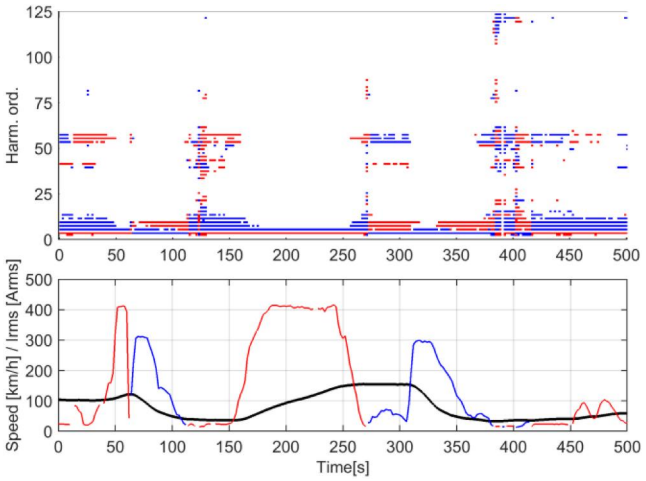

FIGURE 3 Distribution of largest P_h values (98% percentile) and relation of P_h with speed (black) and I_{rms} for the Swiss 16.7 Hz system (traction = red, braking = blue)

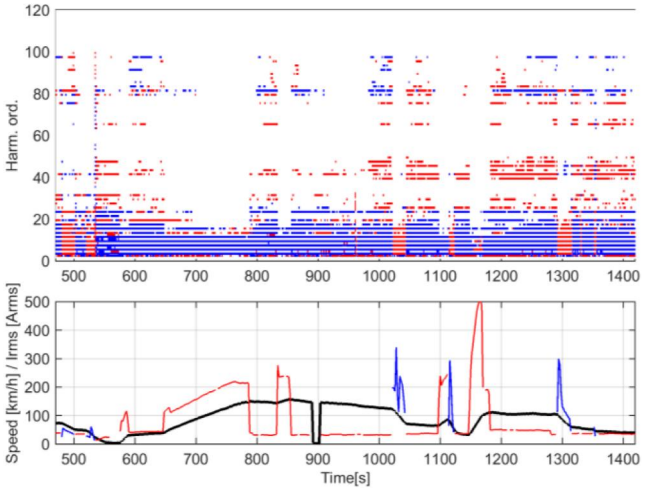

FIGURE 4 Distribution of largest P_h values (95% percentile) and relation of P_h with speed (black) and I_{rms} for the German 16.7 Hz system (traction = red, braking = blue)

harmonics become relevant in low-load conditions during coasting and standstill.

Figure 4 shows the behaviour of another 16.7 Hz system (Germany), that is different, with more intense low-order harmonics and the 4QC components appearing between the 41st and the 55th harmonic (after having selected the 95% percentile for display purposes). The second 4QC group may be observed around the 80th order, possibly mixed with other contributions. As expected, the P_h relevance for the 4QC terms is higher in time intervals with low traction effort. For low-order harmonics it is peculiar that P_h reverses its sign entering the rolling stock during braking, as already observed for the Swiss system in Figure 3.

Figure 5 shows P_h versus I_{rms} and speed for the 50 Hz system.

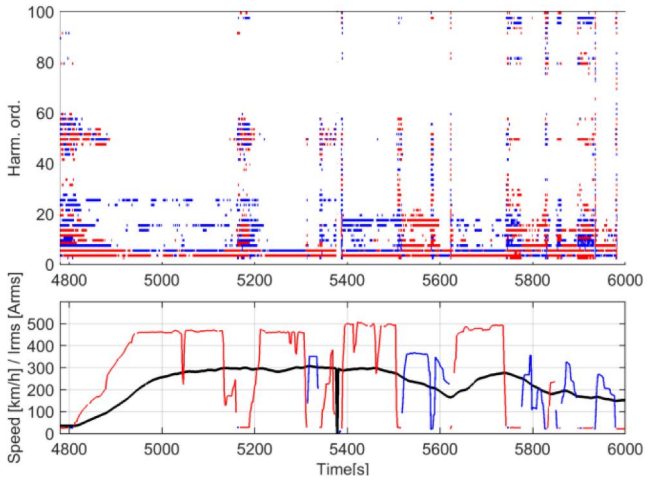

FIGURE 5 Distribution of largest P_h values (95% percentile) and relation with speed (black) and I_{rms} for the French 50 Hz system (traction = red, braking = blue)

TABLE 1 Correlation coefficient of P_h with I_1 and speed s (Swiss 16.7 Hz system)

Harmonic	$\rho(I_1)$	$\rho_{LB}(I_1)$	$\rho_{UB}(I_1)$	$\rho(s)$	$\rho_{LB}(s)$	$\rho_{UB}(s)$
2	–0.008	–0.035	0.019	0.017	–0.01	0.044
3	0.495	0.475	0.515	0.445	0.423	0.466
5	–0.867	–0.873	–0.860	–0.284	–0.308	–0.259
7	0.128	0.102	0.155	–0.192	–0.218	–0.166
41	0.054	0.027	0.081	–0.264	–0.289	–0.239
43	–0.003	–0.030	0.024	0.162	0.136	0.188
45	0.107	0.081	0.134	0.067	0.040	0.093
47	0.004	–0.023	0.0311	0.0138	–0.013	0.041
49	0.014	–0.013	0.041	0.061	0.034	0.088
51	0.090	0.063	0.116	0.083	0.056	0.101
53	0.125	0.098	0.151	0.055	0.028	0.081
55	0.214	0.188	0.239	0.033	0.006	0.060
57	0.196	0.170	0.222	0.091	0.064	0.117
77	0.086	0.059	0.112	0.129	0.103	0.156
79	0.031	0.005	0.058	–0.074	–0.101	–0.047
81	–0.095	–0.122	–0.069	–0.057	–0.084	–0.030
119	0.017	–0.009	0.044	0.132	0.106	0.158
121	0.030	0.003	0.056	0.133	0.106	0.159

In Figure 5, the initial low-speed coasting interval before 4800 s is characterised by low order harmonics up to 25th and higher order harmonics between 45th and 57th. The same repeats for the mixed cruising/coasting at higher speed (300 kmph) that can be observed before 5200 s: it is worth underlying that when passing from cruising to coasting P_h for some of the high-order harmonic changes its sign. At full traction, there are only a few relevant components, namely the third and fifth. The run contains several transients that the tagging algorithm detected as neither traction nor braking (blank segments of the I_{rms} curve) and that are characterised by a burst of several components. There are two P_h components (15th and 17th) that appear with variable amplitude related to the 4QC operation. At about 5 kHz what was interpreted as a line resonance is visible, excited by transients and during coasting phases.

TABLE 2 Correlation coefficient of Q_h with I_1 and speed s (Swiss 16.7 Hz system)

Harmonic	$\rho(I_1)$	$\rho_{LB}(I_1)$	$\rho_{UB}(I_1)$	$\rho(s)$	$\rho_{LB}(s)$	$\rho_{UB}(s)$
2	0.052	0.026	0.079	0.061	0.034	0.088
3	–0.695	–0.709	–0.681	–0.492	–0.512	–0.472
5	0.061	0.034	0.087	–0.162	–0.188	–0.136
7	0.055	0.028	0.082	–0.063	–0.089	–0.036
41	0.161	0.135	0.187	–0.027	–0.053	0.0002
43	–0.215	–0.241	–0.190	–0.234	–0.259	–0.209
45	–0.122	–0.148	–0.095	–0.262	–0.287	–0.237
47	0.011	–0.016	0.038	–0.214	–0.239	–0.188
49	–0.042	–0.069	–0.015	–0.063	–0.089	–0.036
51	–0.024	–0.051	0.003	–0.074	–0.101	–0.048
53	–0.219	–0.244	–0.193	–0.094	–0.121	–0.068
55	–0.075	–0.102	–0.049	0.109	0.082	0.135
57	–0.201	–0.227	–0.175	–0.115	–0.142	–0.089
77	–0.102	–0.129	–0.076	–0.283	–0.307	–0.258
79	–0.025	–0.052	0.0014	0.0057	–0.021	0.033
81	0.079	0.053	0.106	–0.070	–0.096	–0.043
119	–0.016	–0.043	0.011	–0.086	–0.113	–0.060
121	–0.015	–0.042	0.012	–0.093	–0.119	–0.066

5.2 | Correlation with traction effort and speed

Since speed and I_{rms} curves replicate approximately the concept of traction effort, it is interesting to quantify the correlation with the power flow quantities (P_h and Q_h, and the non-active power N_t). With low distortion, for the purpose of correlation, I_{rms} may be exchanged with I_1: for those quantities that show a sign reversal (P_h and Q_h), the intensity I_1 bears its sign, positive when entering the rolling stock; for N_t it is indicated with the absolute value.

A normalised correlation coefficient ρ is calculated, for which the lower and upper bound values ρ_{LB} and ρ_{UB} are also given for the 95% confidence interval of an assumed Gaussian distribution (see Tables 1–3 for the Swiss 16.7 Hz system and Tables 4–6 for the French 50 Hz system).

TABLE 3 Correlation coefficient of N_t with I_1 and speed s (Swiss 16.7 Hz system)

$\rho(\lvert I_1 \rvert)$	$\rho_{LB}(\lvert I_1 \rvert)$	$\rho_{UB}(\lvert I_1 \rvert)$	$\rho(s)$	$\rho_{LB}(s)$	$\rho_{UB}(s)$
0.237	0.211	0.262	0.316	0.292	0.340

TABLE 4 Correlation coefficient of P_h with I_1 and speed s (French 50 Hz system)

Harmonics	$\rho(I_1)$	$\rho_{LB}(I_1)$	$\rho_{UB}(I_1)$	$\rho(s)$	$\rho_{LB}(s)$	$\rho_{UB}(s)$
2	–0.006	–0.036	0.025	–0.023	–0.053	0.007
3	0.286	0.258	0.313	0.025	–0.005	0.055
5	–0.256	–0.2834	–0.227	–0.292	–0.320	–0.265
7	0.342	0.3151	0.368	0.237	0.209	0.266
9	0.322	0.2951	0.349	0.204	0.175	0.233
11	0.073	0.0433	0.103	0.045	0.015	0.075
13	–0.115	–0.1445	–0.085	–0.036	–0.066	–0.006
15	–0.171	–0.2003	–0.142	–0.090	–0.120	–0.060
17	–0.080	–0.1095	–0.050	–0.112	–0.142	–0.083
19	0.026	–0.0039	0.056	0.019	–0.011	0.049
21	0.063	0.0328	0.093	0.122	0.093	0.152
45	–0.023	–0.0528	0.007	0.005	–0.025	0.035
47	–0.035	–0.0644	–0.004	–0.054	–0.084	–0.024
49	–0.154	–0.1829	–0.124	–0.147	–0.176	–0.118
51	–0.010	–0.0401	0.020	–0.064	–0.094	–0.034
53	0.089	0.0588	0.118	0.084	0.054	0.114
55	–0.019	–0.0489	0.011	0.062	0.032	0.092
97	0.107	0.0773	0.137	0.054	0.024	0.084

TABLE 5 Correlation coefficient of Q_h with I_1 and speed s (French 50 Hz system)

Harmonics	$\rho(I_1)$	$\rho_{LB}(I_1)$	$\rho_{UB}(I_1)$	$\rho(s)$	$\rho_{LB}(s)$	$\rho_{UB}(s)$
2	0.0093	–0.0207	0.0393	–0.0245	–0.0545	0.0056
3	0.4498	0.4255	0.4735	0.2675	0.2394	0.2952
5	0.2983	0.2707	0.3254	0.2236	0.1949	0.252
7	0.0006	–0.0294	0.0306	0.0112	–0.0188	0.0412
9	0.0282	–0.0018	0.0582	0.0092	–0.0208	0.0392
11	–0.0027	–0.0327	0.0274	–0.0672	–0.097	–0.0372
13	–0.0022	–0.0322	0.0278	–0.0604	–0.0903	–0.0305
15	0.0237	–0.0064	0.0537	0.0177	–0.0124	0.0477
17	–0.0227	–0.0527	0.0074	0.0198	–0.0103	0.0498
19	–0.0288	–0.0588	0.0012	–0.0351	–0.065	–0.005
21	–0.0021	–0.0321	0.028	–0.082	–0.1117	–0.052
45	0.0942	0.0643	0.1238	0.0823	0.0524	0.112
47	0.0035	–0.0266	0.0335	–0.0385	–0.0684	–0.0085
49	–0.0396	–0.0695	–0.0095	–0.0858	–0.1155	–0.0559
51	–0.0745	–0.1043	–0.0446	–0.1915	–0.2203	–0.1624
53	0.0252	–0.0048	0.0552	–0.049	–0.0789	–0.019
55	0.0522	0.0222	0.0821	0.047	0.017	0.0769
97	0.1152	0.0855	0.1448	0.1055	0.0757	0.1351

TABLE 6 Correlation coefficient of N_t with I_1 and speed s (French 50 Hz system)

$\rho(\lvert I_1 \rvert)$	$\rho_{LB}(\lvert I_1 \rvert)$	$\rho_{UB}(\lvert I_1 \rvert)$	$\rho(s)$	$\rho_{LB}(s)$	$\rho_{UB}(s)$
0.309	0.281	0.336	0.099	0.069	0.129

It is interesting to observe the significant correlation of the fifth harmonic for P_h, rather than for Q_h, supporting the idea that P_h is an effective harmonic power indicator, despite the inconsistency in some cases identified in the past for three-phase systems [25,26]. For Switzerland, the consistent value of P_h, although smaller than a widely varying Q_h value, is confirmed in Figures 6 and 7.

P_h at 4QC frequencies is small and this is also confirmed by a stronger correlation of Q_h for 43rd and 45th components. A stronger correlation is observed for the 53rd, 55th and 57th components that carry both active and reactive power. All these components belong to the 4QC modulation pattern centred on the 48th (800 Hz), with modulation by-products spreading up to 150 Hz from it.

The overall distortion in terms of total non-active power N_t is considered in Table 3: the selection of speed s rather than I_1 is important in boosting the correlation value as the N_t quantity is a non-negative one, whereas I_1 was selected to replicate the direction of current with sign reversal.

Table 3 confirms that the non-active harmonic power N_t is related to the traction/braking effort, higher for larger intensity of the fundamental, although the relationship is not proportional and higher N_t percentages are observed at low current intensity due to auxiliaries (the correlation coefficient is in fact only 0.25). The reason for a higher correlation with speed is the different way cruising and coasting are accounted for: they are characterised by low current intensity, large distortion and a moderate to high speed value (that numerically is more relevant).

The correlation is calculated again for a different case, the French 50 Hz system, and results shown in Tables 4–6.

It is evident that the harmonic power terms are poorly correlated with the o.c., with only low-order harmonics up to the ninth showing significant values. The non-active power N_t is significantly correlated to the fundamental I_1 as expected, but scarcely correlated to the speed, simply because the French run was characterised by high–speed cruising with limited braking and traction phases (high-speed train).

It is in general understood that straightforward correlation has the drawback of being influenced by numeric values and that two different systems are thus hardly comparable. In reality, correlation and similarity operated on normalized quantities, such as the sign of P_h, P_h, are more effective.

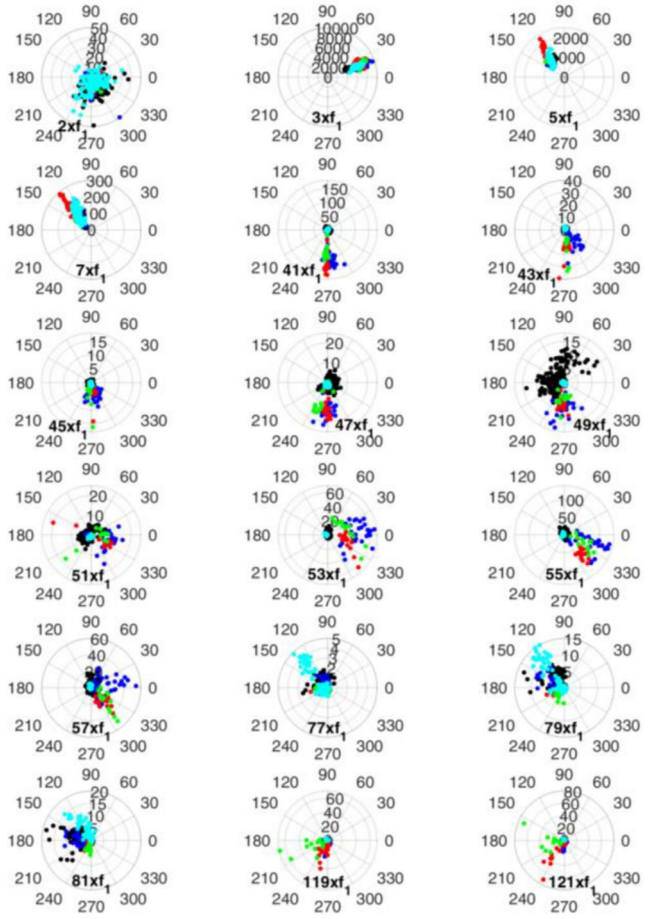

FIGURE 6 P_h–Q_h polar diagram for CH 16.7 Hz harmonics: traction condition, five different time intervals (colour)

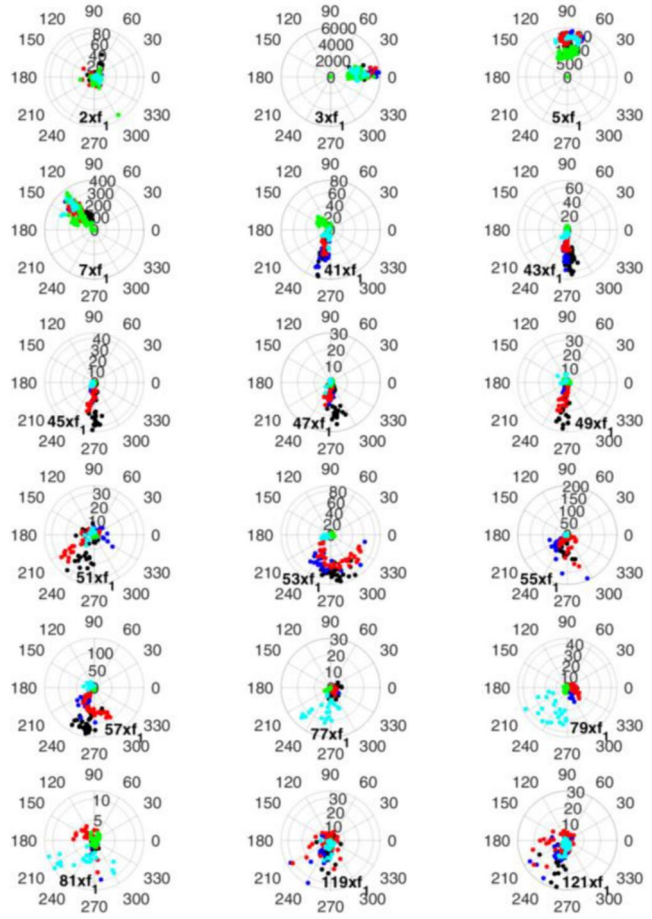

FIGURE 7 P_h–Q_h polar diagram for CH 16.7 Hz harmonics: braking condition, five different time intervals (colour)

5.3 | Harmonic power displacement factor

The pair P_h–Q_h corresponds to the harmonic displacement factor d_h, but bears also information of intensity. It is displayed at various characteristic harmonics during selected t.i. of traction, braking and coasting o.c.. Results are shown in the following having selected significant cases: Figures 6–9 for 16.7 Hz systems, Figures 10 and 11 for the 50 Hz system. As anticipated, the harmonic reactive power Q_h is defined and calculated for common terms to V_h and I_h.

The P_h–Q_h plots lend themselves to the application of clustering, to assess the level of coherence between sets of samples belonging to the same o.c. In this analysis, clusters are displayed with different colours and their characteristics are visually assessed for simplicity.

For both 16.7 Hz systems, the second harmonic is confirmed not correlated as it has an almost circular shape with arbitrary phase relationships, quite similar for the three o.c. For Switzerland, the fifth and seventh have similar distribution for the various intervals and the three o.c. These three components are related to network distortion originating from the substation, since if caused by other rolling stock they would not be stationary. For Germany, the fifth and seventh are coherent for braking and coasting, but show a significant dispersion (especially the fifth) during traction.

For the third harmonic (for both Switzerland and Germany), the intervals for the same o.c. are in strong agreement, but different o.c. have a consistently different behaviour, although the change of angle and amplitude is not dramatic: a significant third harmonic originates from the on-board transformer nonlinearity and it is thus correlated with I_1 and I_{rms}, but it is also due to the auxiliaries (working at 50 Hz), whose operation is almost independent on the traction conditions.

For Switzerland, the 51st to 57th show a consistent change of angle passing from traction (Figure 6) to braking (Figure 7) with the P_h part passing from positive to negative, although there is prevalence of Q_h. In coasting, o.c. components are all of negligible amplitude, confirming that they are related to the operation of the traction converter of the Re460. Conversely, the 41st to 47th harmonics keep an almost unchanged pattern between traction and braking, leading to suppose external network origin (in coasting, they spread and reduce their amplitude as the loco input impedance gets larger).

For Germany, the 45th, 47th and 65th components show a remarkable compactness with a constant displacement

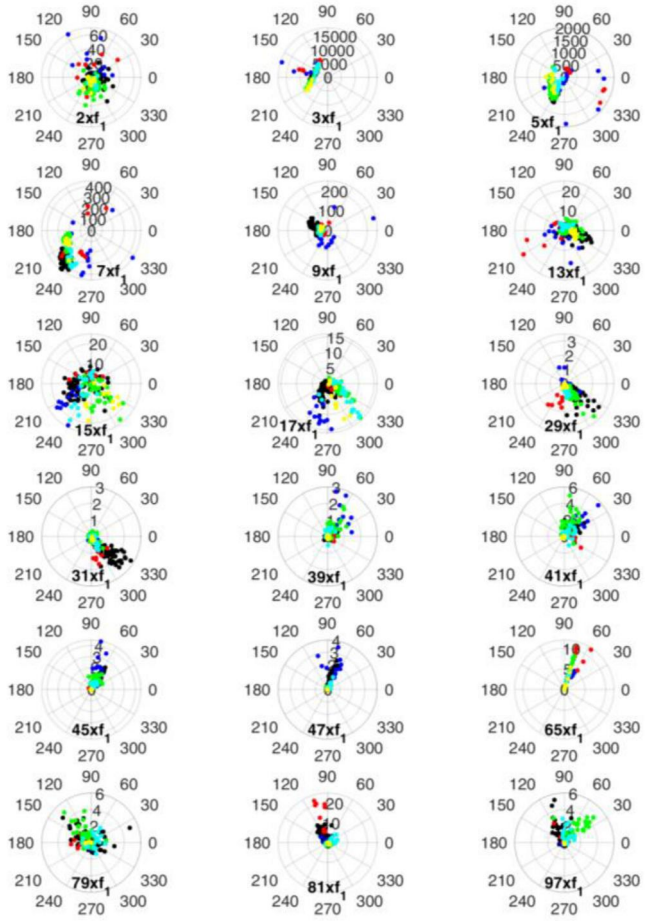

FIGURE 8 P_h–Q_h polar diagram for D 16.7 Hz harmonics: traction condition, six different time intervals (colour)

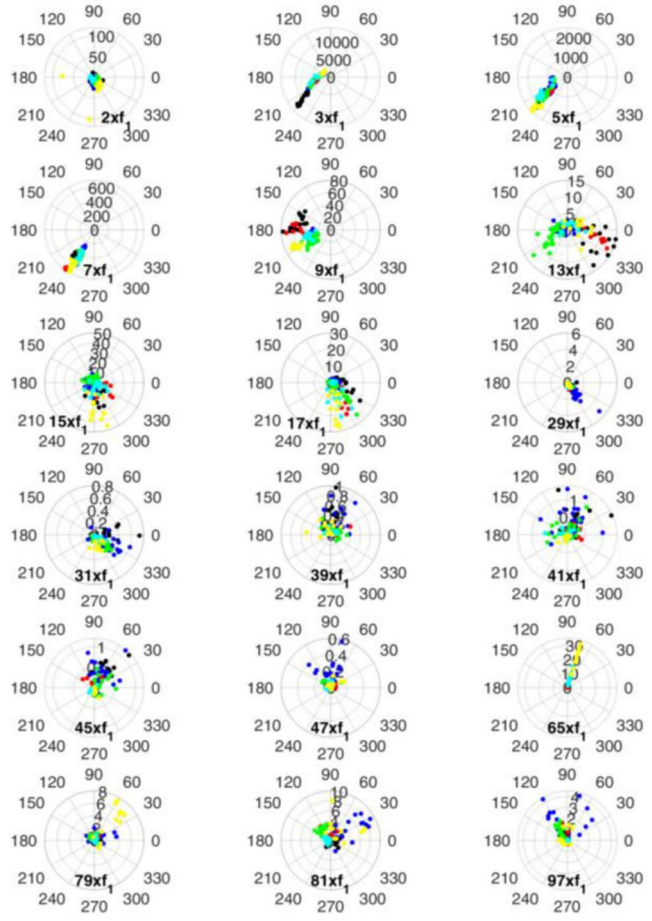

FIGURE 9 P_h–Q_h polar diagram for D 16.7 Hz harmonics: braking condition, six different time intervals (colour)

angle and limited spread throughout traction and braking, slightly larger for braking o.c., indicating an external origin. Conversely, low-order harmonics have significant change of phase between the two o.c., suggesting correlation to the train o.c., confirmed also by the significant amount of low-frequency P_h terms shown in Figure 4.

For the 50 Hz system considered in Figures 10 and 11, there is significant compactness for P_h–Q_h values of harmonics between 9th and 21st: values are almost overlapped for different time intervals in the same o.c. (traction and braking) and also between o.c. In coasting, values are slightly more dispersed and one-two orders of magnitude smaller, demonstrating that these components are related to the traction converter. This is sensible considering that the Dasye has naturally commutated input rectifiers with GTO power factor control operating at low switching frequency.

For the 97th harmonic, there is a significant dispersion between o.c. and between t.i., although within the same time interval values are sufficiently compact, hinting origin from other rolling stock with consistent o.c. in short t.i. (the amplitude values are all quite small). For harmonics between 45th and 55th, the values show a large dispersion again not correlated to o.c. and within the same t.i., apparently indicating again external origin, although there is a substantial presence of larger values for traction o.c. (possibly because the loco input impedance is smaller).

5.4 | Complex harmonic diagrams

In Ref. [18], converter components were displayed using scatter plots in the real-imaginary plane. The resulting circular pattern is not peculiar of converter modulation but of all harmonics that undergo unavoidably a phase rotation with an approximately constant amplitude over short time intervals. As shown in Figure 12, both network and converter harmonics feature the mentioned circular pattern. The second harmonic, known to be unrelated to loco o.c., shows a broken diagram, and similarly the third at low I_1 current (black), again weakly related to I_1 and traction o.c. It is observed that the seventh shares the same shape of known converter harmonic (51st, 53rd and 55th), both in terms of dispersion and somewhat dependency on I_1 (although green is the innermost but red is

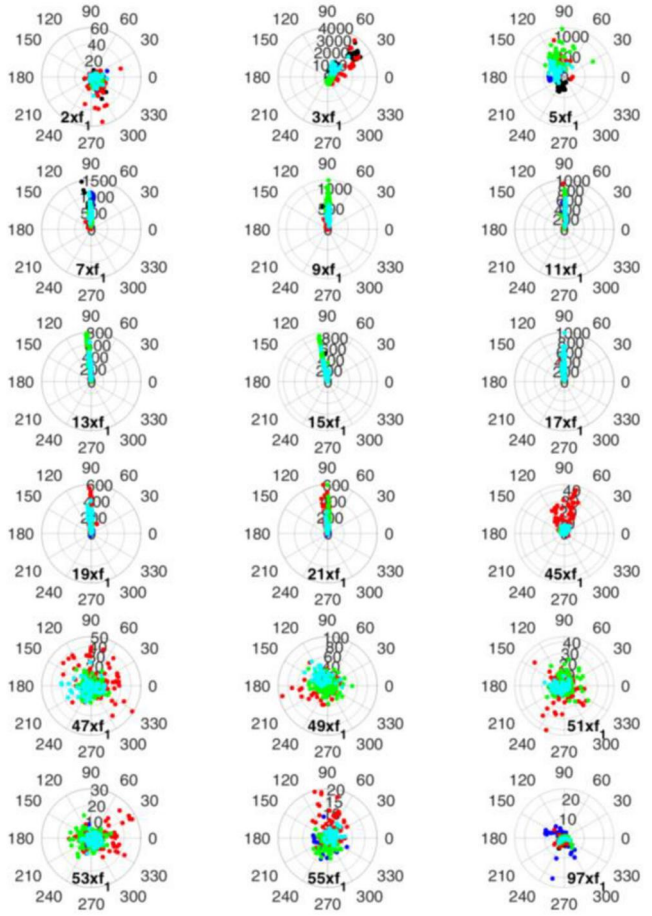

FIGURE 10 P_h–Q_h polar diagram for F 50 Hz harmonics: traction condition, five different time intervals (colour)

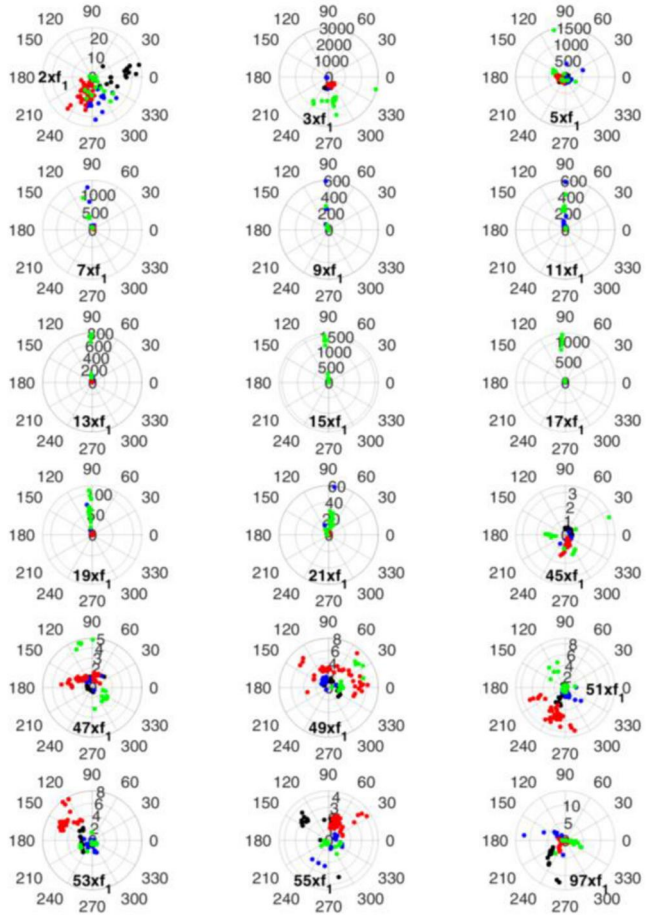

FIGURE 11 P_h–Q_h polar diagram for F 50 Hz harmonics: braking condition, four different time intervals (colour)

the outermost, so the dependency is not monotonic). Slightly more dispersed patterns can be seen for the 79th and 119th that are known to belong to other rolling stock on the same supply section.

The Re–Im plots of current harmonics are not a strong indicator of the origin of harmonic distortion terms, being the slightly larger dispersion of components from external converters a bit subjective. However, low-order network components are more easily distinguishable thanks to apparently irregular patterns.

6 | CONCLUSION

Pantograph voltage and current recorded along three major European railways (Switzerland, Germany and France) have been subject to analysis of harmonic patterns and active and non-active harmonic power terms. Several time intervals were extracted with almost constant operating conditions (within traction, braking and coasting phases) to study clustering and similarity of patterns and correlation with effort and speed.

The objective was to quantify the amount of active and reactive power for non-fundamental terms and to explore algorithms and methods applicable to quantities measured only at the pantograph interface for the identification of harmonic terms of internal and external origin.

The most direct application is to metering and accounting of consumed and utilised energy, defining first the minimum frequency range of energy metres to include relevant distortion power terms and also supporting fair billing, by distinguishing power terms of internal and external origin. It was in fact demonstrated [4,14] that harmonic active power is relevant to the calculation of the total energy consumption in particular compared to the uncertainty target. Similarly, such methods may be used to assess the distortion provided by the network attempting to quantify its spectral P and Q, rather than V and I components separately. Both have a direct relationship with recent standardisation works of EN 50,463-2 and EN 50388.

The implementation on existing energy metres would be not demanding since available hardware is able to acquire and process low-order harmonics (resulting the most relevant from this analysis), although presently limited to the fundamental for compliance to standard.

The identified characteristics for the power terms at the low-order harmonics and for those related to converter commutation at higher orders are repeatable and represent a first set of rules. Low-order harmonics are generally external network terms, although the third harmonic is related to the

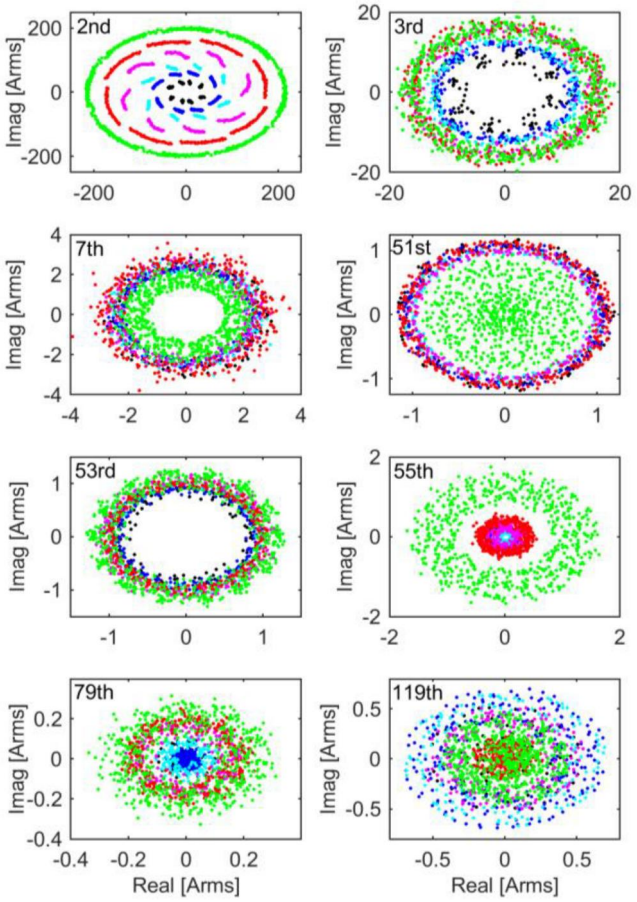

FIGURE 12 Real–Imag diagrams of harmonic current I_h for varying I_1 during traction (CH 16.7 Hz): I_1 = 30 (black), 60 (blue), 90 (cyan), 130 (mag.), 170 (red), 210 (green) Arms

input transformer and for 16.7 Hz systems to the 50 Hz fundamental of auxiliaries. Converter emissions may be first identified observing the current vector in the real-imaginary plane. The first characteristic emission pattern of traction converters is generally located between about 500 and 2000 Hz, depending on technology. Separation of own and external components can be achieved by evaluating the dispersion of P_h and Q_h scatter plots during intervals of constant operating conditions.

Traditional single-point PQ indicators have been investigated in Ref. [26] for application to AC railways, showing that harmonic active power (API) and direction of flow are the best indicators compared with those based on harmonic distortion power. Such API quantity may be backed up by information on P_h-Q_h phase dependency and correlation with operating conditions, to confirm internal origin of harmonic components.

The future development of this work is towards a more quantitative assessment of spread and similarity of graphical patterns: for example clustering techniques based on K-means or K-median and their variants, that can be improved to include Gaussian Mixture Models and expectation-maximisation algorithms; or unsupervised techniques, such as density-based DBSCAN and OPTICS. A thorough verification of consistency and performance should be based on much larger datasets (above the four to five vectors selected here for each o.c.) and considering a wider range of rolling stock types.

ACKNOWLEDGEMENTS

The results here presented were developed in the framework of the 16ENG04 MyRailS Project and the European Union's Horizon 2020 research and innovation program. This work was supported by the Swiss State Secretariat for Education, Research and Innovation (SERI) under contract number 17.00127. The opinions expressed and arguments employed herein do not necessarily reflect the official views of the Swiss Government.

REFERENCES

1. Said, D.M., Nor, K.M., Majid, M.S.: Analysis of distribution transformer losses and life expectancy using measured harmonic data. Proc. 14th Intern. Conf. Harm. Qua. Pow. (ICHQP), Bergamo, Italy, September 26-29, 2010
2. Wang, J., et al.: Harmonic loss analysis of the traction transformer of high-speed trains considering pantograph-OCS electrical contact properties. Energies. 6, 5826–5846 (2013)
3. Mariscotti, A.: Characterisation of active power flow at harmonics for AC and DC railway vehiclesIn: Proc. IEEE Veh. Pow. Prop. Conf., Hanoi, Vietnam, Oct., vol. 14-17 (2019)
4. Mariscotti, A.: Impact of harmonic power terms on the energy measurement in AC railways. IEEE Trans. Instrum. Meas. 69(6), 6731–6738 (2020)
5. Mariscotti, A.: Behaviour of spectral active power terms for the Swiss 15 kV 16.7 Hz railway system, In: Proc. 10th IEEE Intern. Workshop on Applied Meas. for Pow. Sys., Aachen, Germany, September 25-27, 2019
6. Lee, K.D., et al.: Estimation of variable-speed-drive power consumption from harmonic content. IEEE Trans. Energy Conv. 20(3), 566–574 (2005)
7. Mirchevski, S., et al., Significance of non-active power in energy efficiency of electric drives. In: X intern. Conf. On Electr. Pow. Drive Sys. (ICEPDS). Novocherkassk, Russia. 3–6 October 2018
8. Chang, G.W., Lin, H.W., Chen, S.K.: Modelling characteristics of harmonic currents Generated by high-speed railway traction drive converters. IEEE Trans. Power. Del. 19(2), 766–773 (2004)
9. Brenna, M., et al.: Current distortion evaluation in traction 4Q constant switching frequency converters. J. Electrom. Anal. Appl. 3, 129–137 (2009)
10. Agamloh, E.B.: 'Power and efficiency measurement of motor-variable-frequency drive systems. IEEE Trans. Ind. Appl. 53(1), 766–773 (2017)
11. Mariscotti, A., Ruscelli, M., Vanti, M.: Modeling of Audiofrequency Track Circuits for validation, tuning and conducted interference prediction. IEEE Trans. Intel. Transp. Syst. 11(1), 52–60 (2010)
12. Dolara, A, Gualdoni, M., Leva, S.: EMC disturbances on track circuits in the 2×25kV high speed AC railways systems. In: IEEE PowerTech, Trondheim, Norway. 19–23 June 2011
13. Railway applications – energy measurement on board trains, Report No. EN 50463-2. (2017)
14. Mariscotti, A.: Uncertainty of the energy measurement function deriving from distortion power terms for a 16.7 Hz railway. Acta Imeko. 9(2), 25–31 (2020)
15. Richter, M., Komarnicki, P., Hauer, I.: Improving state estimation in smart distribution grid using synchrophasor technology: a comparison study. Arch. Elec. Eng. 67(3), 469–483 (2018)
16. Pegoraro, P.A., et al.: 'Line impedance estimation based on synchrophasor measurements for power distribution systems. IEEE Trans. Instrum. Meas. 68(4), 1002–1013 (2019)
17. Zhang, J., Shang, J., Zhang, Z.: Optimization and control on high frequency resonance of train-network coupling systems. Math. Probl. Eng., 1–10 (2019)

18. Hu, H., et al.: Power-quality impact assessment for high-speed railway Associated with high-speed trains using train timetable – Part I: Methodology and modelling. IEEE Trans. Power Del. 31(2), 693–703 (2016)
19. Hasegawa, D., et al.: Standardised approach to energy consumption calculations for high-speed rail. IET Electr. Syst. Transp. 6(3), 179–189 (2015)
20. Frey, D., et al.: Study of high frequency harmonics propagation in industrial networks. In: Proc. IEEE Intern. Symp. Electrom. Comp., pp. 1–5.Italy, Rome (2012)
21. Rönnberg, S. K., et al.: On waveform distortion in the frequency range of 2-150 kHz – Review and research challenges. Electric Power Syst. Res. 150, 1–10 (2017)
22. Hemmer, B., Mariscotti, A., Wuergler, D.: Recommendations for the calculation of the total disturbing return current from electric traction vehicles. IEEE Trans. Power Del. 19(2), 1190–1197 (2004)
23. Mariscotti, A.: 'Data sets of measured pantograph voltage and current of European AC railways', Data In Brief, 30, 105477, pp. 1-12, 2020
24. IEEE standard definitions for the measurement of electric power quantities under sinusoidal, nonsinusoidal, balanced, or unbalanced condition, Report No. IEEE Std. 1459. (2010)
25. Barbaro, P.V., et al.: A novel approach based on nonactive power for the identification of disturbing loads in power systems. IEEE Trans. Power Del. 22(3), 1782–1789 (2007)
26. Mariscotti, A.: Behaviour of single-point harmonic producer indicators in electrified AC railways. Metrol. Meas. Syst. (in print)
27. Railway Applications – power supply and rolling stock – Technical criteria for the coordination between power supply (substation) and rolling stock to achieve interoperability, Report No. EN 50388. (2013)
28. Railway Applications – Fixed installations and rolling stock – Technical criteria for the coordination between traction power supply and rolling stock to achieve interoperability – Part 1: General, Report No. prEN 50388-1. (2017)
29. Boschetti, G., Mariscotti, A.: Integrated electromechanical simulation of traction systems: relevant factors for the analysis and estimation of energy efficiency, Proc. Intern. Conf. Elec. Sys. Aircraft, Railway Ship Prop. (ESARS), Bologna, Italy, 16-18 October, 2012
30. Bigharaz, M. H., et al.: A comprehensive simulator of AC autotransformer electrified traction system. Int. J. Power Energy Conv. 10(2), 129–147 (2019)
31. Mariscotti, A.: Results on the power uality of French and Italian 2x25 kV 50 Hz railways.Proc. IEEE intern. Instrum. Meas. Techn. Conf. (I2MTC). Graz, Austria (13–16 May 2012)

How to cite this article: Mariscotti A. Experimental characterisation of active and non-active harmonic power flow of AC rolling stock and interaction with the supply network. *IET Electr. Syst. Transp*. 2021;1–12. https://doi.org/10.1049/els2.12009